

# **Copper and Nitrogen co-doped TiO<sub>2</sub> photocatalyst with enhanced optical absorption and catalytic activity**

**R. Jaiswal<sup>a</sup>, J. Bharambe<sup>a</sup>, N. Patel<sup>\*,a,b</sup>, Alpa Dashora<sup>a</sup>, D.C. Kothari<sup>a</sup> and A. Miotello<sup>b</sup>**

<sup>a</sup> *Department of Physics and National Centre for Nanosciences & Nanotechnology, University of Mumbai, Vidyanagari, Santacruz (E), Mumbai 400 098, India*

<sup>b</sup> *Dipartimento di Fisica, Università degli Studi di Trento, I-38123 Povo (Trento), Italy*

**\* Corresponding author: Nainesh Patel,**

**Tel. No.:** +39-0461882012

**Fax No.:** +39-0461881696

**e-mail address:** patel@science.unitn.it, nainesh11@gmail.com

## **Abstract**

Cu-N-codoped TiO<sub>2</sub> photocatalyst is synthesized by sol-gel method to obtain enhanced optical absorption in the visible region. Optimum concentrations of Cu and N were obtained by maximizing the photocatalytic activity for the monodoped (Cu or N) TiO<sub>2</sub>. These optimized concentrations were used for synthesizing (Cu, N)-codoped TiO<sub>2</sub>. The photocatalysts were characterized using XRD, micro-Raman, SEM, XPS, BET surface area analyzer, UV-Visible diffuse reflectance spectroscopy and Photoluminescence. XPS study suggests the incorporation of Cu<sup>2+</sup> into TiO<sub>2</sub> lattice, which assists N to substitutionally replace oxygen in codoped TiO<sub>2</sub>,

while maintaining the anatase phase even after doping. N-doping creates minor variation in the energy band gap of TiO<sub>2</sub> reducing it upto 3.0 eV, while Cu doping was able to narrow the band gap to 2.2 eV mainly due to the localized levels of Cu-3d states and shifting of Ti-3d states to lower energy (due to oxygen vacancies) in the band-gap as deduced from XPS data and confirmed by the DFT calculation. In (Cu, N)-codoped TiO<sub>2</sub>, visible light absorption is higher than the other TiO<sub>2</sub> samples, a feature that is mainly attributed to the formation of an isolated intermediate band (IB) occurring due to the strong hybridization between Cu 3d and N 2p orbitals. This IB contributes to visible light absorption by two step optical transition with the first transition from valence band (VB) to IB and the second from IB to conduction band (CB). The dopant species may also act to reduce the radiative recombination by acting as the trapping sites for photogenerated charges. (Cu, N)-codoped TiO<sub>2</sub> was able to degrade Methylene Blue dye and p-Nitrophenol solution under light irradiation with significantly better rate in comparison to monodoped and undoped TiO<sub>2</sub>. High photocatalytic activity is attributed to the presence of IB in the energy band gap of TiO<sub>2</sub>, which creates the synergic effect by higher visible light absorption and lower recombination of photogenerated charges.

**Keywords:** Photocatalytic degradation, Codoped TiO<sub>2</sub>, Sol-gel method, Intermediate band, Methylene blue, p-Nitrophenol.

### **Introduction:**

Titanium dioxide (TiO<sub>2</sub>) shows high photocatalytic activity among the semiconductor photocatalysts that have been investigated for the elimination of organic pollutants in aqueous or in the gas phase [1]. In addition, high chemical stability, environmental friendliness, easy availability, and cost effectiveness makes TiO<sub>2</sub> an ideal candidate as a photocatalyst [2]. Unfortunately, TiO<sub>2</sub> displays photoactivity only under UV light (wavelength <400 nm) due to its wide band gap (3.2 eV for anatase crystalline phase). Since the fraction of UV in the solar spectrum on the earth's surface is less than 5%, it is important to sensitize TiO<sub>2</sub> photocatalyst

to absorb visible light which would result in efficient utilization of the main part of the solar spectrum [3]. Therefore, increasing the efficiency of visible light absorption of TiO<sub>2</sub> is a subject of extensive current research. The previous research works provided some promising methods to enhance the photoactivity of TiO<sub>2</sub>, involving metal or non-metal ions doping and co-doping [4].

Doping with metals like Cr, Fe, V, Mn, Cu, Zn, Ni [5-8] reduces the energy band gap of TiO<sub>2</sub> and simultaneously reduces the recombination rate of photogenerated electron-hole pairs. However, at higher dopant concentrations these metals themselves become the cause of the recombination of photogenerated electrons and holes [9]. Doping TiO<sub>2</sub> with non-metallic anions such as N, S, and C, replaces O in the TiO<sub>2</sub> lattice to generate energy levels just above the top of the valence band of TiO<sub>2</sub> thus narrowing the band gap [10, 11]. Even though, the band gap is narrowed to a certain extent by low concentration monodoping (p-type or n-type), this narrowing is not enough for the efficient use of visible light. At higher concentration doping, it was experimentally observed that the impurity levels act as charge recombination center and reduce the photo-activity [4].

Recently, the concept of second generation TiO<sub>2</sub> based materials was introduced where co-doping with two dopant elements produces a synergic effect to enhance the visible light absorption efficiency and reduce the recombination processes of the photogenerated charges [12-23]. Zhu et al. [12] have described a new idea of non-compensated n-p codoping which generates intermediate band (IB) in the mid gap of TiO<sub>2</sub> and increases both the thermodynamic stability and kinetics of dopants. Cr and N codoping was used as a model for non-compensated n-p codoping which showed increased visible light absorption and charge separation. Gai et al. [13] theoretically demonstrated that codoping of TiO<sub>2</sub> with passivated codopants such as Mo and C in charge-compensated condition shifts the Valance Band Maximum (VBM) up significantly, while leaving Conduction Band Minimum (CBM) almost unchanged to satisfy

the condition for hydrogen reduction in water splitting process. Several other combination of dopants such as V-N, Cr-C, Fe-N, Zr-N, Si-Ni etc.[14-18] have been studied in the past for various photocatalytic applications. Most researchers concentrated on codoping of metal and non-metal species where the former serves as n-type dopant while the later as p-type dopant. In this scenario, the dopants either produce charge compensation or provide net n- or p-type charge carriers. However, very few theoretical or experimental works are presented in literature where p-type metal is codoped with non-metal which also serves as p-type dopant. Metal species such as  $\text{Cu}^{2+}$ ,  $\text{Ni}^{2+}$ ,  $\text{Co}^{3+}$ , and  $\text{Fe}^{3+}$  contribute charge carriers in the form of holes to convert  $\text{TiO}_2$  from n-type semiconductor to p-type [19-20]. Song et al. [21] and Wang et al. [22] prepared (Cu, N)-codoped  $\text{TiO}_2$  nanoparticles and investigated the influence of the amounts of Cu and N co-doped into  $\text{TiO}_2$  on the photocatalytic activity. Co-doping of  $\text{TiO}_2$  with N and Cu extends the absorption band up to 590 nm and produces higher photocatalytic activity than the pure N- or Cu-doped  $\text{TiO}_2$  for the degradation of organic pollutants. In our recent article [23], the theoretical calculations carried out for *p*-type codoping of Cu and N in  $\text{TiO}_2$  revealed the presence of an isolated in (IB) deep in the band gap due to strong hybridization between Cu 3d and N 2p orbitals. The new IB is mostly responsible for high visible light absorption through a two-step optical transition. Nevertheless, experimental evidence is necessary in proving the ability of this codoped  $\text{TiO}_2$  to be used as an efficient photocatalyst material.

The present work focuses on one of the second generation  $\text{TiO}_2$  based materials, namely, (Cu, N)-codoped  $\text{TiO}_2$ , for its use in the photocatalytic degradation of organic pollutants from the aqueous media. The synthesis route used is sol-gel and the enhanced photocatalytic activity observed for (Cu, N)-codoped  $\text{TiO}_2$  is discussed in terms of synergic effects produced by the presence of IB in its energy band gap.

## Experimental methods:

Sol-gel method was used to synthesize pure TiO<sub>2</sub> by using titanium (IV) butoxide (Ti(OCH<sub>2</sub>CH<sub>2</sub>CH<sub>2</sub>CH<sub>3</sub>)<sub>4</sub>) and nitric acid (HNO<sub>3</sub>) as precursor and catalyst respectively. Molar ratio of Ti (OC<sub>4</sub>H<sub>9</sub>)<sub>4</sub>/H<sub>2</sub>O/ethanol/HNO<sub>3</sub> was kept constant at 1/30/20/0.1. Ethanol(C<sub>2</sub>H<sub>5</sub>OH) and the precursor were mixed for 1 hour (hr) at room temperature to form homogeneous mixture. Similarly, another solution mixture of de-ionized water, ethanol and HNO<sub>3</sub> was prepared under constant stirring. Later, water based solution was added drop wise into Ti precursor solution under constant stirring for 1 hr. To enhance the homogeneity, the resulting solution was further stirred for 1 hr at constant speed. To prepare N-doped TiO<sub>2</sub> triethylamine (N(CH<sub>2</sub>CH<sub>3</sub>)<sub>3</sub>) was mixed with precursor, while for Cu-doped TiO<sub>2</sub> hydrated copper nitrate (II) was dissolved in water based solution. Procedure used for Cu and N doping was combined to synthesized (Cu, N)-codoped TiO<sub>2</sub>. For gelation, the resulting solution was left overnight at room temperature followed by drying at 100 °C for 3 hr to remove excess solution. After grinding the resulting powder were calcined in air at 500 °C for 2 hr. Sample nomenclature used in the present work is shown in Table 1.

The surface morphology of all the samples was studied by Scanning Electron Microscope (SEM-FEG, JSM 7001F, JEOL) equipped with Energy-Dispersive Spectroscopy analysis (EDS, INCA PentaFET-x3) to determine the composition of the samples. The structural characterization of the all samples was performed by X-ray diffraction (XRD) using Cu K<sub>α</sub> radiation ( $\lambda = 1.5414 \text{ \AA}$ ). Raman spectra were recorded by using Renishaw micro-Raman spectrometer (RE-04) using solid state laser with the diode pumped at 514 nm. The band gap of the doped TiO<sub>2</sub> was determined by measuring the UV-Vis absorption spectra (taken in diffuse reflectance mode), using Cary 500 UV-Vis-NIR spectrophotometer, in the range of 200 nm to 800 nm. The surface composition and chemical states of the samples were

examined by X-ray photoelectron spectra using a SCIENTA ESCA200 instrument equipped with a monochromatic Al  $K_{\alpha}$  (1486.6eV) X-ray source and a hemispherical analyzer. No electrical charge compensation was necessary to perform the analysis. Single point BET surface area of the powder photocatalysts was determined by nitrogen absorption at 77 K (Smart SORB 93) after degassing at 120 °C for 2 hrs. Photoluminescence (PL) study was carried out using Fluorescence Spectrophotometer (Varian; Cary Eclipse) where emission spectra were collected by exciting the photocatalyst with wavelength of 385 nm. To acquire PL spectra 3 mg of powder photocatalyst was dispersed in aqueous medium of fixed amount and transferred into 1 cm x 1 cm cuvette for measurement.

The photocatalytic activity of all the samples was evaluated by photodegradation of 0.01 mM methylene blue (MB) dye solution under light irradiation. 150 W Xenon lamp (Philips), which has spectrum nearly similar to solar spectrum, was used as the source of light. Photocatalytic degradation experiment was carried out using 50 ml of aqueous MB solution containing 20 mg of photocatalyst. The powder suspension was stirred for 30 min in dark to attain adsorption-desorption equilibrium of the molecules in the solution. The distance between the beaker and the light source was kept constant at 10 cm. After established time intervals, 1 ml MB aqueous solution was filtered out from the reactor vessel. The UV-visible adsorption spectra of the filtered solution were measured using the spectrophotometer. The photocatalytic activity was determined by measuring the normalized intensity of the absorption band of MB at 665 nm and plotting it as a function of time of irradiation (Figure S1 of supporting information). All the photocatalysis experiments were performed at room temperature and the pH of the solution was neutral during all the photocatalytic measurements. Similar type of experiment and measurement was performed for the degradation of transparent p-nitrophenol (p-NP) aqueous solution (10 ppm) where the absorption band at 320 nm was monitored with respect to time (Figure S2 of supporting information).

## Results and discussion:

In order to use the optimized concentration of Cu and N for codoping, TiO<sub>2</sub> was mono-doped with Cu or N using three different concentrations. As determined from the EDS analysis, the Cu atomic concentrations were approximately 0.5, 1, 2 at.% whereas those of N were 1, 2, 3 at.% in TiO<sub>2</sub> for different samples. Low concentrations were used for doping because at high concentrations the same dopants behave as recombination sites for photogenerated charges thus decreasing the catalytic activity. The XRD patterns of TiO<sub>2</sub> mono-doped with Cu or N are presented in Fig. 1 along with the undoped TiO<sub>2</sub>. The peaks observed at  $2\theta$  of 25.3°, 37.7°, 48.1°, 53.8°, and 55.1° in all the powder samples correspond to (101), (004), (200), (105), and (211) planes of anatase phase [4]. This shows that the doping at low concentrations preserves the initial anatase structure of TiO<sub>2</sub>. The grain size calculated from the prominent peak of anatase phase (101) at  $2\theta = 25.3^\circ$  is in the range of 10-15 nm (Table 1) for all the TiO<sub>2</sub> samples, thus suggesting nano-crystalline structure of the TiO<sub>2</sub>. In the case of Cu-doped TiO<sub>2</sub>, the position of main anatase peak at  $2\theta = 25.3^\circ$  shifts to higher  $2\theta$  value as compared to pure TiO<sub>2</sub> (inset Fig. 1). This indicates that Cu was incorporated in the TiO<sub>2</sub> network and the slightly bigger size of Cu<sup>2+</sup> ion (0.087 nm) than Ti<sup>4+</sup> ion (0.075 nm) may have caused the variation in dimension of lattice [8]. Any other possible peaks due to copper oxide or copper metal are not observed in the XRD pattern.

Optical properties of Cu- or N-doped TiO<sub>2</sub> were studied using UV-Vis spectroscopy by measuring optical spectra in the range of 200-800 nm, in diffuse reflectance mode. Tauc plot of  $(\alpha h\nu)^{1/2}$  vs  $(h\nu)$  (Fig. 2) was used to evaluate the band gap energies by extrapolating the linear region of the plot to intersect the photon energy axis; the obtained values are summarized in Table 1. For pure TiO<sub>2</sub>, the band gap value of 3.15 eV was obtained, which is close to the expected value of the anatase phase (3.2 eV). After N-doping, the band gap of

TiO<sub>2</sub> decreases to 3.0 eV for the highest concentration. On the other hand, significant narrowing of band gap was observed after Cu-doping and the band gap value decreases with the increase in dopant concentration. For the highest Cu concentration (2 at. %) the band gap decreases to 2.2 eV. The reasons for these major variations in the band gap are discussed later.

To test the photoactivity, the degradation of MB dye was examined as a function of time in the presence of Cu-doped and N-doped TiO<sub>2</sub> powders under light irradiation. The decrease of MB dye concentration was estimated by measuring the relative intensity of the peak at 665 nm from the optical absorbance spectra. Very low amount of self degradation of MB was observed under the light irradiation in the absence of photocatalyst. In the presence of TiO<sub>2</sub> powder, the degradation rate was fairly noticeable; all the samples (doped and undoped) were able to convert the blue color solution into colorless solution (100% degradation). Fig. 3 presents the time taken by TiO<sub>2</sub> to completely degrade MB dye, as a function of N and Cu dopant atomic concentration. Irrespective of the doping concentration, the N-doped and Cu-doped TiO<sub>2</sub> showed photocatalytic activity higher than the undoped TiO<sub>2</sub>. As the doping concentrations increase, the photocatalytic activity increases and shows maximum for highest doping concentration (i.e. 2 at. % for Cu and 3 at.% for N). Most significantly, Cu-doped TiO<sub>2</sub> displays considerably better activity as compared to the N-doped samples. On the basis of these results, the dopant concentrations of 2 at. % for Cu and 3 at. % for N were selected for co-doping to perform additional studies. Henceforth this sample is designated as 2Cu-3N-TiO<sub>2</sub>.

Structural modifications induced both at the surface and in the bulk of TiO<sub>2</sub> after codoping were studied by using Raman spectroscopy (Fig. 4) and XRD (Fig. 5) respectively. As observed in Fig. 4 Raman peaks centered at 144, 197, 399, 513, and 639 cm<sup>-1</sup> are attributed to the E<sub>g</sub>, E<sub>g</sub>, B<sub>1g</sub>, A<sub>1g</sub>, and B<sub>2g</sub> modes, respectively, of the anatase phase of TiO<sub>2</sub> [24]. This indicates that the anatase phase is preserved on the surface after monodoping as well as codoping of Cu and N. XRD patterns (Fig. 5) show that the bulk of 2Cu-3N-TiO<sub>2</sub> powder



contains all the major peaks assigned to the anatase phase. An additional peak at  $27.4^\circ$  is also observed for the codoped  $\text{TiO}_2$  which is attributed to rutile phase. ~~Rearrangement of  $\text{TiO}_2$  network due to codoping is mainly responsible for the rutile phase formation~~ In codoped  $\text{TiO}_2$ , bigger size  $\text{Cu}^{2+}$  (0.087 nm) replaces the  $\text{Ti}^{4+}$  (0.075 nm) sites which produces strain energy by lattice distortions, while  $\text{N}^-$  replaces  $\text{O}^{2-}$  ions creating oxygen deficiency in  $\text{TiO}_2$  lattice. Both these features allow the rearrangement of  $\text{Ti}^{4+}$  and  $\text{O}^{2-}$  ions in the lattice to favour the anatase to rutile phase transformation [9]. SEM images of pure  $\text{TiO}_2$ ,  $2\text{Cu-TiO}_2$ ,  $3\text{N-TiO}_2$ , and  $2\text{Cu-3N-TiO}_2$  powders are presented in Fig. 6. Undoped- $\text{TiO}_2$  exhibits particle like morphology with irregular spherical shape with average particle size of  $\sim 650$  nm.  $3\text{N-TiO}_2$  also displays spherical particles but with size ( $\sim 120$  nm) much smaller than undoped  $\text{TiO}_2$ . On the contrary, big irregular crystallites of 1-5  $\mu\text{m}$  are observed for  $3\text{Cu-TiO}_2$ . In the case of  $2\text{Cu-3N-TiO}_2$  sample, spherical particles are present with average particle size of  $\sim 310$  nm which is higher than that of the N-doped  $\text{TiO}_2$  but lower than that of the pure  $\text{TiO}_2$ . Surface area, measured by single point BET method using  $\text{N}_2$  absorption, decreases in following order:  $3\text{N-TiO}_2$  ( $88 \text{ m}^2/\text{g}$ )  $>$   $2\text{Cu-3N-TiO}_2$  ( $65 \text{ m}^2/\text{g}$ )  $>$   $\text{TiO}_2$  ( $27 \text{ m}^2/\text{g}$ )  $>$   $2\text{Cu-TiO}_2$  ( $7 \text{ m}^2/\text{g}$ ). The obtained trend is attributed to the particle size of these photocatalyst powders. This shows that after Cu-doping the particle-like morphology of  $\text{TiO}_2$  is completely lost while, on the contrary, it is again restored after co-doping with N, thus demonstrating the advantage of the codoping in maintaining the morphology. Elemental mapping using EDS were carried out to examine the spatial distribution of elements in co-doped  $\text{TiO}_2$  (Fig. 7). All the elements namely, Ti, O, N, and Cu, were detected and uniformly distributed. Colored spots assigned to Cu and N elements indicate that both dopants are well mixed in the  $\text{TiO}_2$  network.

Chemical states of each element in undoped  $\text{TiO}_2$ ,  $2\text{Cu-TiO}_2$ ,  $3\text{N-TiO}_2$  and  $2\text{Cu-3N-TiO}_2$  photocatalysts were examined by XPS and are reported in Figure 8. In  $\text{Ti}2\text{p}$  core level, both N-doped and pure  $\text{TiO}_2$  samples display peaks at 458.7 eV and 464.5 eV assigned to Ti

$2p_{3/2}$  and Ti  $2p_{1/2}$  of  $Ti^{4+}$  states [25]. After Cu doping both these peaks appear to be very broad. After deconvolution of the Ti  $2p_{3/2}$  signal into two peaks, it is observed that the peak due to  $Ti^{4+}$  is positively shifted by 0.3 eV to 459 eV as compared to the Ti  $2p_{3/2}$  peak of undoped  $TiO_2$ . This signifies that Cu is incorporated into  $TiO_2$  lattice, in agreement with XRD result, and influences the local chemical state of  $Ti^{4+}$  ions [26]. Another deconvoluted peak centered at 456.8 eV attributed to  $Ti^{3+}$  is also present with ratio of 1:2 versus  $Ti^{4+}$  species thus suggesting the presence of higher amount of oxygen vacancies in the  $TiO_2$ . Since  $Cu^{2+}$  or  $Cu^+$  ions having lower oxidation states replace  $Ti^{4+}$  ions having higher oxidation state, the energy required to form oxygen vacancies in Cu-doped  $TiO_2$  is significantly lower than undoped  $TiO_2$  [27]. The peak at 456.6 eV due to  $Ti^{3+}$  is significantly suppressed in Cu-N-codoped  $TiO_2$  indicating the major decrease in O-vacancies mainly due to the presence of N which fills these vacancies substitutionally. O1s level displays the peak (530 eV) due to oxygen bonded in  $TiO_2$  with small peak due to the adsorbed  $O_2$  (532 eV) [28] in pure  $TiO_2$  and N-doped  $TiO_2$  samples. Additional peak at 527.5 eV obtained after deconvolution is assigned to the oxygen in Cu-O bond [29], which is seen in the O1s peak of Cu-doped and codoped  $TiO_2$  samples. While investigating Cu2p core level, it is inferred that Cu is present only in  $Cu^{2+}$  state with corresponding peaks at 934.7 and 953.6 eV of Cu  $2p_{3/2}$  and Cu  $2p_{1/2}$  states, respectively [30], for both 2Cu- $TiO_2$  and 2Cu-3N- $TiO_2$  samples. Even the characteristic satellite peak (942 eV) of  $Cu^{2+}$  is observed due to the shake-up transition by a ligand-metal 3d charge transfer [8]. In N1s core level, a broad peak is deconvoluted into two peaks centered at 400.7 eV and 399.5 eV in the case of Cu-N-codoped  $TiO_2$ . The former peak arises due to N substitutionally replacing oxygen to form O-Ti-N linkage while later peak is due to interstitial occupation of N and oxidized N species (NO) to form Ti-O-N and Ti-O-N-O linkage respectively [31]. However, for N-monodoped  $TiO_2$ , only single peak related to interstitial N is observed. These results show that for codoped  $TiO_2$ , Cu is present in form of  $Cu^{2+}$  species in  $TiO_2$  lattice whose

presence also forces N to substitutionally replace oxygen in the lattice. Even though the peak shift in XRD pattern and XPS spectra prove that  $\text{Cu}^{2+}$  species are incorporated into  $\text{TiO}_2$ , the possible presence of CuO species on the photocatalyst surface cannot be discarded owing to the chemical route used for the synthesis. The dopant concentration obtained by XPS analysis for the doped- (2.79 at. % for 3N- $\text{TiO}_2$  and 1.91 at. % for 2Cu- $\text{TiO}_2$ ) and codoped- $\text{TiO}_2$  (2.85 at. % of N and 1.82 at. % of Cu for 2Cu-3N- $\text{TiO}_2$ ) are in good agreement with that obtained by EDS analysis.

Diffuse reflectance was measured for pure  $\text{TiO}_2$ , 3N- $\text{TiO}_2$ , 2Cu- $\text{TiO}_2$  and 2Cu-3N- $\text{TiO}_2$  using UV-Vis spectroscopy. Tauc plot was used to determine the band gap of these samples (Fig. 9). After mono-doping the band gap value decreases to 3.0 eV and 2.2 eV for 3N- and 2Cu- $\text{TiO}_2$  powder respectively. However, for the co-doped powder (2Cu-3N- $\text{TiO}_2$ ) the absorption edge is not properly defined and decreases continuously in lower energy range. Thus, the lack of linear region in the Tauc plot makes it very difficult to obtain the exact value of the band gap energy. Nevertheless, the absorption edge is at lower energy than 2Cu- or 3N-monodoped  $\text{TiO}_2$  and the band gap value is roughly estimated to be below 2.0 eV.

In order to understand the major variation in the band gap of  $\text{TiO}_2$  after doping, theoretical calculation was performed using Density Function Theory (DFT) with modified Beck-Jhonson potential. Details of the calculation with obtained results are reported in our recent article [23] while here we briefly describe the relevant results. Major contribution to VBM and CBM due to O-2p and Ti-3d states, respectively, is inferred from the PDOS (Fig. 2 of ref. [23]) of pure  $\text{TiO}_2$ . Energy bands (Fig. 2 of ref. [23]) of  $\text{TiO}_2$  reveal a direct band gap of 3.2 eV at  $\Gamma$  point and indirect band gap of 2.9 eV in  $\Gamma$ -N branch. For N-  $\text{TiO}_2$ , localized state are formed just above the O-2p states by N 2p states and shifts the VBM to higher energy by 0.1 eV whereas CBM also shifts to lower value by 0.3 eV with respect to pure  $\text{TiO}_2$ . Both these features are able to decrease the band gap of N-doped  $\text{TiO}_2$  by small amount (0.4 eV) as

in agreement with experimentally measured band gap for 3N-TiO<sub>2</sub>. In the case of Cu-doped TiO<sub>2</sub>, the isolated levels are formed at 0.3 eV above the VBM due to the Cu-3d orbital. However, major shift (0.9 eV) in CBM towards lower energy is observed for Cu-doped TiO<sub>2</sub>. As demonstrated by XPS, noticeable amount of O-vacancies are formed by Cu doping by replacing Ti<sup>4+</sup> with Cu<sup>2+</sup>/Cu<sup>1+</sup> in the lattice and these vacancies are responsible for the major shift in the CBM by forming localized states. In order to confirm this feature, a separate calculation based on DFT was performed by introducing O vacancies in pure TiO<sub>2</sub> which showed exactly similar lowering in the CBM in agreement to the results presented by Sotoudeh et al. [32]. Theoretically, band gap decreases by 1.2 eV for Cu-doped TiO<sub>2</sub> which is in good agreement with the experimentally obtained narrowing of 2Cu-TiO<sub>2</sub> (2.2 eV). In addition to the localized state formed above the VBM by N 2p and Cu 3d states, an additional isolated (IB) is observed for Cu-N-TiO<sub>2</sub>. This IB is dominated by the Cu 3d orbitals and located 0.72 eV above the VBM and 1.14 eV below the CBM. The existence of this IB is attributed to the strong hybridization between the Cu 3d and N 2p orbitals creating new energy levels deep in the band gap. Thus the absence of well defined absorption edge in Fig. 9 for codoped TiO<sub>2</sub> is mainly due to the presence of IB. This IB contributes in visible light absorption by two step optical transitions with the first transition from VB to IB of about 1.0 eV and the second transition from IB to CB by absorbing 1.6 eV photons. These results show that codoping induces strong hybridization between Cu and N to form IB deep in the band gap to absorb high amount of visible light as compared to monodoped TiO<sub>2</sub>. Unlike Cu-monodoped TiO<sub>2</sub>, the shift in CBM towards lower energy is very less for the codoped TiO<sub>2</sub> (0.3 eV) which is mainly attributed to the decrease in O vacancies as observed by the XPS results. This shows that the hybridization between Cu and N is very strong to form N-Cu-O bond in the TiO<sub>2</sub> network to decrease the density of O vacancies.

Photoluminescence (PL) spectra in TiO<sub>2</sub> originate from the radiative recombination of photogenerated charges. Thus this information can be used to understand the recombination process. Fig.10 presents the emission peaks in violet (420, 438 nm), blue (485 nm) and green (526, 547 nm) regions for all the undoped, monodoped and co-doped TiO<sub>2</sub> samples. The first set of peaks at 420 nm and 438 nm occur by relaxation of self trapped excitons generated through the transition along the band edges [33]. While the rest of the peaks 485, 526 and 547 nm are present due to the intra band transitions within the energy level traps or surface defects [34]. Compared with pure TiO<sub>2</sub>, there is reduction in emission intensity for Cu- or N-doped TiO<sub>2</sub> and intensity is further decreased for Cu-N-codoped TiO<sub>2</sub>. This shows that upon doping and codoping the radiative recombinations of charge carrier is considered to be decreased due to its trapping in the dopant sites.

The photocatalytic activity of 2Cu-3N-TiO<sub>2</sub> was compared with the monodoped (2Cu-TiO<sub>2</sub> and 3N-doped TiO<sub>2</sub>) and undoped-TiO<sub>2</sub> for photodegradation of MB dye (Fig. 11). The codoped TiO<sub>2</sub> shows much higher catalytic activity and is able to complete the reaction with less amount of time in comparison to the other samples. The time required for codoped TiO<sub>2</sub> to produce colorless solution (100% degradation) is 2.9, 1.7, and 1.3 times lower than that required by TiO<sub>2</sub>, 3N- TiO<sub>2</sub>, and 2Cu-TiO<sub>2</sub>, respectively. In order to test the degradation of p-Nitrophenol, the photocatalytic powder was immersed in p-Nitrophenol solution of 10 ppm. By analyzing the peak at 320 nm, the amount of degradation was studied as a function of time and reported in Fig. 12. After 2 hrs, codoped-TiO<sub>2</sub> was able to degrade 45 % of p-NP which is considerably higher than 2Cu-TiO<sub>2</sub> (29 %), 3N-TiO<sub>2</sub> (26 %), and pure TiO<sub>2</sub> (18 %). The data points in Fig. 11 and Fig. 12 were fitted linearly to calculate apparent rate constant and, RhB and n-NP degradation rate per gram of photocatalyst and are summarized in Table 2.

Degradation of organic pollutants such as MB and p-NP takes place through the action of the strong oxidizing agents (O<sub>2</sub><sup>•-</sup> and OH<sup>•</sup> radicals) produced by photogenerated electrons

and holes in TiO<sub>2</sub> from absorbed O<sub>2</sub> and H<sub>2</sub>O [35]. If this mechanism is true than three main factors, namely surface area of the photocatalyst (useful for interaction with dye, H<sub>2</sub>O and O<sub>2</sub> molecules), light absorption capability (as more photons are absorbed, more charge carriers are produced), and charge separation or transfer (oxidizing agent such as O<sub>2</sub><sup>•-</sup> and OH<sup>•</sup> are produced only if e<sup>-</sup> and h<sup>+</sup> are efficiently separated to have time to travel to the surface of photocatalyst and interact with dye, H<sub>2</sub>O and O<sub>2</sub> molecules ) are of paramount importance for the efficient degradation reaction. High surface area in codoped TiO<sub>2</sub> can be effective in increasing the absorption of the reactants on the active sites as compared to pure and Cu-doped TiO<sub>2</sub>. However, N-doped TiO<sub>2</sub> exhibits the highest surface area but the activity is lower than the 2Cu-3N-TiO<sub>2</sub> suggesting that the surface area is not the major reason for the enhancement. Ability to absorb high amount of visible light by the doped TiO<sub>2</sub> is the most important factor that is responsible for the observed advanced catalytic activity. Significant narrowing of the band gap for Cu-doped TiO<sub>2</sub>, due to the formation of isolated energy levels of Cu above VBM and shift of CBM to lower energy due to of O-vacancies is accountable for the higher photocatalytic activity in Cu-doped TiO<sub>2</sub> as compared to the N-doped TiO<sub>2</sub>. In the case of Cu-N-TiO<sub>2</sub>, along with the decrease in the band gap, an isolated IB is also formed by strong hybridization between the Cu 3d and N 2p orbitals. IB contributes to absorb photons of lower energy by allowing two step transitions of excited electrons moving from VB to IB and from IB to CB. The increased efficiency in visible light photons absorption, as confirmed by UV-vis spectra, contributes for the high number production of e<sup>-</sup> and h<sup>+</sup> pairs thus increasing the degradation rate of organic molecule for codoped TiO<sub>2</sub>. However to achieve effective degradation, these photo-generated charges must have time, before recombination, to travel to the surface for the generation of oxidizing agents. In this context, the energy level formed above the VBM by N dopant act as a hole trapping sites due to the charge imbalance between oxygen and nitrogen in N-doped TiO<sub>2</sub>. This phenomenon is more effective when N

substitutionally replaces oxygen in the TiO<sub>2</sub> lattice as in case of Cu-N-codoped TiO<sub>2</sub> where the presence of Cu<sup>2+</sup> species forces N to occupy substitutional sites as observed by XPS. In the case of Cu-doped TiO<sub>2</sub>, Cu<sup>2+</sup> ions can trap not only holes but also electrons. As indicated by the theoretical calculations, the energy levels formed by Cu<sup>2+</sup> species are above the VBM which can act as hole trapping sites. On the contrary, the oxygen vacancies created because of different oxidation states of Ti<sup>4+</sup> and Cu<sup>2+</sup>, shifts the CBM to lower energy that assist in capturing electrons thus promoting separation of photogenerated charges. In addition to both these features of N<sup>2-</sup> and Cu<sup>2+</sup> species for charge separation, the recombination problem can be further reduced in Cu-N-codoped TiO<sub>2</sub> owing to the formation of broadened IB where charge carriers have higher mobility as compared to the localized states produced by mono-doping. PL spectra also suggests that radiative recombination in codoped-TiO<sub>2</sub> may have decreased. Thus increase charge separation is also held liable for the higher activity for the codoped TiO<sub>2</sub>. Concentration of dopants is another parameter that can contribute in the increased photocatalytic activity. In the present case, the optimum level of doping was selected, because for the concentrations above this amount, the same trapping sites may act as the recombination centers, as evident from the photocatalytic activity determined for various concentrations in the case of mono-doped samples.

The above results show that p-type dopants in the form of Cu and N codoped -TiO<sub>2</sub> operate synergistically to increase visible light absorption and charge separation thus resulting in higher photocatalytic activity as compared to pure TiO<sub>2</sub>. IB formed in the band gap also opens up new avenues for utilizing TiO<sub>2</sub> based material for developing intermediate-band-gap solar cell with high quantum efficiency [36]. No major variation in the CBM also guarantees its potential in using it for photocatalytic water splitting for hydrogen generation with high efficiency. In this case indeed the CBM must be above the reducing potential of water to

reduce hydrogen, a condition verified by the present co-doped TiO<sub>2</sub> but not with the present Cu doped and other transition metal doped TiO<sub>2</sub> [13].

### **Conclusions:**

TiO<sub>2</sub> was doped with N, Cu, and codoped with Cu & N to increase visible light absorption and to reduce the recombination of photogenerated charges. It was observed that N-doping creates minor reduction in the band gap of TiO<sub>2</sub> to about 3.0 eV. On the contrary, Cu doping was able to narrow the band gap to a value of 2.2 eV, a result explained on the basis of DFT calculation showing the presence of localized electronic levels of Cu-3d and of oxygen vacancies in the mid-gap. In (Cu, N)-codoped TiO<sub>2</sub>, visible light absorption is higher than in the other TiO<sub>2</sub> samples, a feature that DFT calculation permitted to explain on the basis of an IB formed through hybridization of Cu 3d and N 2p orbitals. This IB contributes to visible light absorption by two steps optical transition from VB to IB and then from IB to CB. Degradation of MB dye and p-NP solution under visible light irradiation proceeds in (Cu, N)-codoped TiO<sub>2</sub> with significantly better rate than in the case of monodoped and undoped TiO<sub>2</sub>. Along with the increase in visible light absorption, the IB contributes to reduction of charge recombination by providing a fast path for electrons transport: both effects contribute synergistically to photocatalytic activity of the Cu-N-codoped TiO<sub>2</sub>.



**Acknowledgement:** We thank Lucia Calliari for XPS analysis and Nicola Bazzanella for SEM analysis. The research activity is partially supported by UGC-UPE Green Technology Project in India and by the PAT (Provincia Autonoma di Trento) project ENAM in cooperation with Istituto PCB of CNR (Italy). One of us (AD) is thankful to SERB-DST, New Delhi, India for Young Scientist Project.

### References:

- [1] A. Fujishima, K. Honda, *Nature* 238 (1972) 37–38.
- [2] T. Bak, J. Nowotny, M.Rekas, C.C.Sorrell, *Int. J. Hydrogen Energy* 27 (2002) 991-1022.
- [3] A. Fujishima, X. Zhang, D.A. Tryk, *Surf. Sci. Rep.* 63 (2008) 515-582.
- [4] R. Jaiswal, N. Patel, D.C. Kothari, A. Miotello, *Appl. Catal. B: Environ.* 126 (2012) 47–54.
- [5] W.Y Choi, A. Termin, M.R. Hoffmann, *J. Phys. Chem.* 84 (1994) 13669–13679.
- [6] M.I. Litter, J.A. Navio, *J. Photochem. Photobiol. A: Chem.* 98 (1996) 171-181.
- [7] R. Dholam, N. Patel, A. Santini, A. Miotello, *Int. J. Hydrogen Energy* 35 (2010) 9581-90.
- [8] R. Lo´pez, R. Go´mez, M.E. Llanos, *Catal. Today* 148 (2009) 103–108.
- [9] R. Dholam, N. Patel, M. Adami, A. Miotello, *Int. J. Hydrogen Energy* 34 (2009) 5337-5346.
- [10] J. Senthilnathan, L. Philip, *Chem. Eng. J.* 161 (2010) 83–92.
- [11] F. Dong, S. Guo, H. Wang, X. Li, Z. Wu, *J. Phys. Chem. C* 115 (2011) 13285–13292.

- [12] W. Zhu, X. Qiu, V. Iancu, X.Q. Chen, H. Pan, W. Wang, N.M. Dimitrijevic, T. Rajh, H.M. Meyer III, M.P. Paranthaman, G.M. Stocks, H.H. Weitering, B. Gu, G. Eres, Z. Zhang, *Phys. Rev. Lett.* 103 (2009) 226401-4.
- [13] Y. Gai, J. Li, S.S. Li, J.B. Xia, S.H. Wei, *Phys. Rev. Lett.* 102 (2009) 036402(1-4).
- [14] N. Patel, R. Jaiswal, T. Warang, G. Scarduelli, A. Dashora, B.L. Ahuja, D.C. Kothari, A. Miotello, *Appl. Catal. B: Environ.* 150–151 (2014) 74–81.
- [15] S. Zhang, *Ultrason. Sonochem.* 19 (2012) 767-771.
- [16] L. Jia, C. Wu, S. Han, N. Yao, Y. Li, Z. Li, B. Chi, J. Pu, L. Jian, *J. of Alloys Compd.* 509 (2011) 6067-6071.
- [17] X. Yao, X. Wang, L. Su, H. Yan, M. Yao, *J. mol. Catal. A: chem.* 351 (2011) 11-16.
- [18] Y. Lin, Z. Jiang, C. Zhu, X. Hu, X. Zhang, H. Zhu, J. Fan, *Apl. catal. Lett.* 101 (2012) 062106.
- [19] M. Hamadani, A. Reisi-Vanani, A. Majedi, *J. Iran. Chem. Soc.* 7 (2010) S52–S58.
- [20] Y.J. Lin, Y.H. Chang, W.D. Yang, B.S. Tsai, *J. Non-Cryst. Solids* 352 (2006) 789–794.
- [21] K. Song, J. Zhou, J. Bao, Y. Feng, *J. Am. Ceram. Soc.* 91 (2008) 1369-1371.
- [22] S. Wang, X.J. Yang, Q. Jiang, J.S. Lian, *Mater. Sci. Semicond. Process.* 24 (2014) 247-253.
- [23] A. Dashora, N. Patel, D.C. Kothari, B.L. Ahuja, A. Miotello, *Sol. Energy Mater. Sol. Cells* 125 (2014) 120–126.
- [24] K. Yanagisawa, J. Owenstone, *J. Phys. Chem. B* 103 (1999) 7781-7787.
- [25] Y. Wu, H. Liu, J. Zhang, F. Chen, *J. Phys. Chem. C* 113 (2009) 14689-14695.
- [26] R. Dholam, N. Patel, A. Miotello, *Int. J. Hydrogen Energy* 36 (2011) 6519-6528.

- [27] S. Duhalde, M.F. Vignolo, F. Golmar, *Phys. Rev. B* 72 (2005) 161313.
- [28] R. Nakamura, T. Tanaka, Y. Nakato, *J. Phys. Chem. B* 108 (2004) 10617–10620.
- [29] A.S. Ethiraj, D.J. Kang, *Nanoscale Res. Lett.* 7 (2012) 70(1-5).
- [30] R. Bechara, A. Aboukais, J.P. Bonnelle, *J. Chem. Soc. Faraday Trans.* 89 (1993) 1257.
- [31] L.Z. Li, H.J. Huang, X. Chen, Z.X. Chen, W.J. Li, D. Ye, X.Z. Fu, *Solid State Chem.* 180 (2007) 2630-2634.
- [32] M. Sotoudeh, S.J. Hashemifar, M. Abbasnejad, *AIP Adv.* 4 (2014) 027129(1-13).
- [33] S. Chen, W. Chu, Y.Y. Huang, X. Liu, D.G. Tong, *Mater. Res. Bull.* 47 (2012) 4514-4521.
- [34] R. Chauhan, A. Kumar, R.P. Chaudhary, *Spectrochim. Acta Part A: Mol. Biomol. Spect.* 98 (2012) 256-264.
- [35] U.G. Akpan, B.H. Hameed, *J. Hazard. Mater.* 170 (2009) 520-529.
- [36] F. Wu, H. Lan, Z. Zhang, P. Cui, *J. Chem. Phys.* 13710 (2012) 4702(1-6).

### **Figure Captions:**

**Figure 1:** XRD patterns of undoped, Cu-doped, and N-doped TiO<sub>2</sub> powders with different dopant concentrations. Inset shows the shift in peak position of anatase phase at 25.3°.

**Figure 2:** Tauc Plot obtained from UV-Vis spectra (taken in diffuse reflectance mode), of undoped, Cu-doped, and N-doped TiO<sub>2</sub> powders with different dopant concentrations.

**Figure 3:** Comparison of photocatalytic degradation of MB under light irradiation in presence of undoped, Cu-doped, and N-doped TiO<sub>2</sub> powders, plotted in terms of the time required to produce colorless solution (100 % degradation) vs molar concentration of the doped species (Lines are drawn to guide the eye).

**Figure 4:** Raman spectra of undoped, 2Cu-doped, 3N-doped, and 2Cu-3N-codoped TiO<sub>2</sub> powders.

**Figure 5:** XRD patterns of undoped, 2Cu-doped, 3N-doped, and 2Cu-3N-codoped TiO<sub>2</sub> powders.

**Figure 6:** SEM images of undoped, 2Cu-doped, 3N-doped, and 2Cu-3N-codoped TiO<sub>2</sub> powders.

**Figure 7:** Elemental mapping of 2Cu-3N-codoped TiO<sub>2</sub> powder obtained by EDS analysis.

**Figure 8:** XPS spectra of Ti2p, O1s, Cu2p and N1s levels of undoped, 2Cu-doped, 3N-doped, and 2Cu-3N-codoped TiO<sub>2</sub> powders.

**Figure 9:** Tauc Plot obtained from UV-Vis spectra (taken in diffuse reflectance mode) of undoped, 2Cu-doped, 3N-doped, and 2Cu-3N-codoped TiO<sub>2</sub> powders.

**Figure 10:** Photoluminescence emission spectra of undoped, 2Cu-doped, 3N-doped, and 2Cu-3N-codoped TiO<sub>2</sub> powders obtained at the excitation wavelength of 385 nm.

**Figure 11:** Comparison of photocatalytic degradation of MB under light irradiation in presence of undoped, 2Cu-doped, 3N-doped, and 2Cu-3N-codoped TiO<sub>2</sub> powders, plotted in terms of the normalized intensity of the absorption band of MB at 665 nm in UV-vis measurements vs irradiation time (Lines are drawn to guide the eye).

**Figure 12:** Comparison of photocatalytic degradation of p-NP under light irradiation in presence of undoped, 2Cu-doped, 3N-doped, and 2Cu-3N-codoped TiO<sub>2</sub> powders, plotted in terms of the normalized intensity of the absorption band of p-NP at 320 nm in UV-vis measurements vs irradiation time (Lines are drawn to guide the eye).

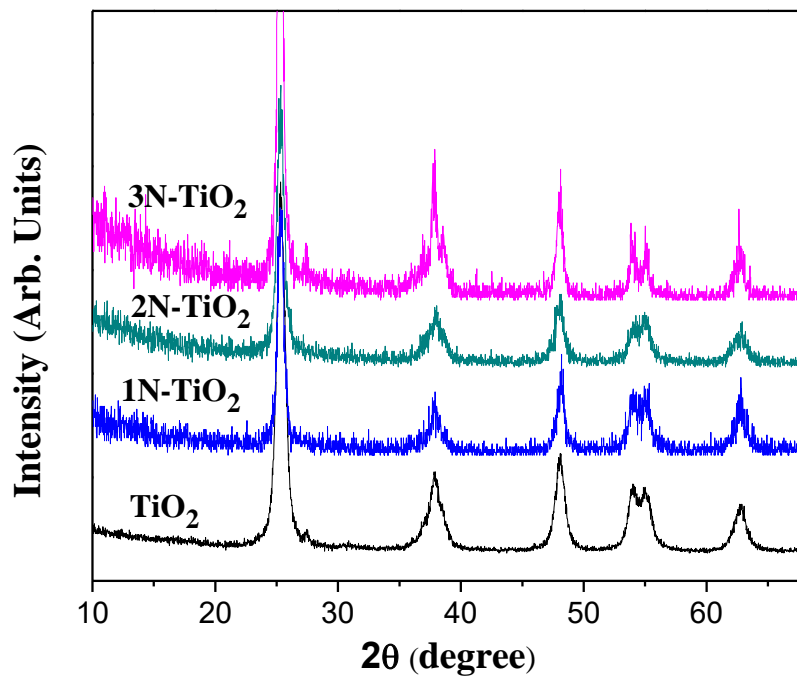
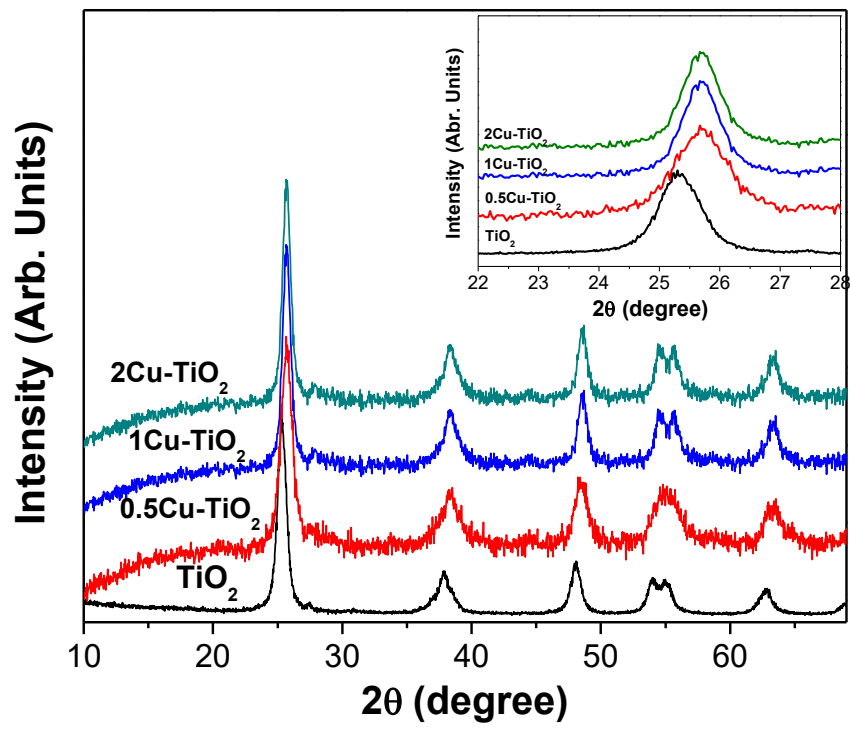


Figure 1:

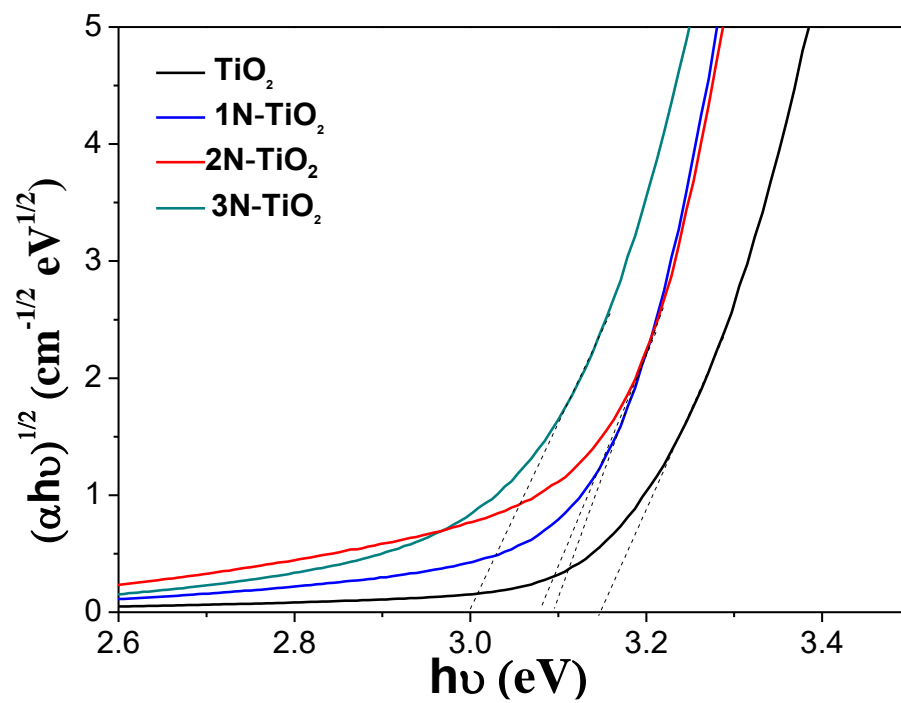
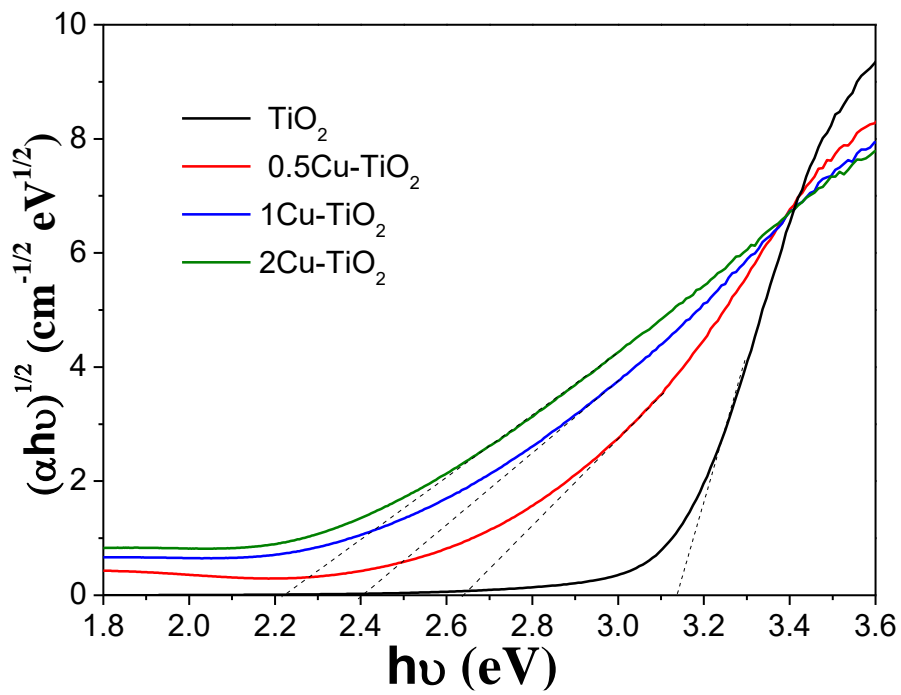
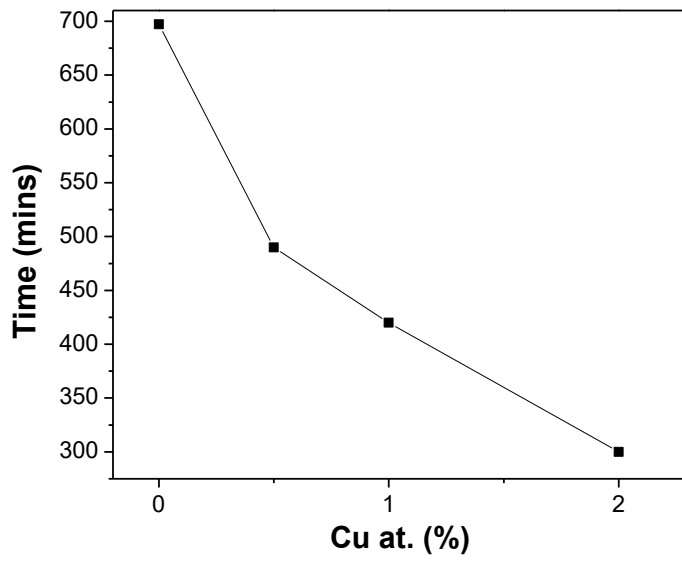
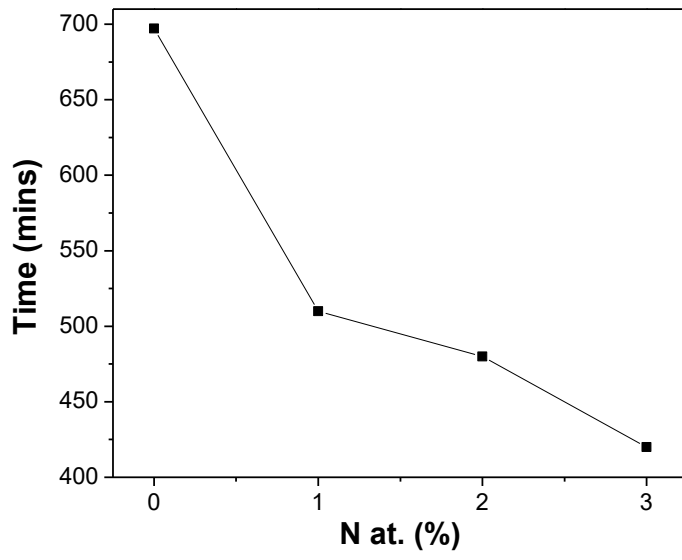


Figure 2:



**Figure 3:**



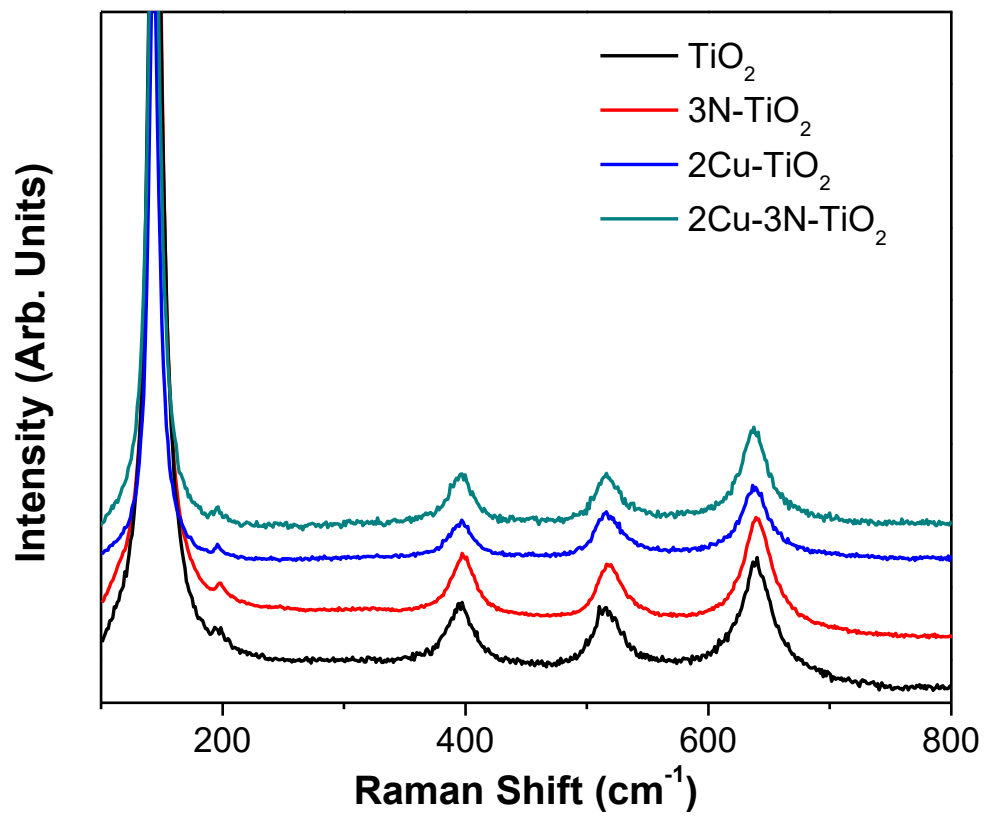


Figure 4:

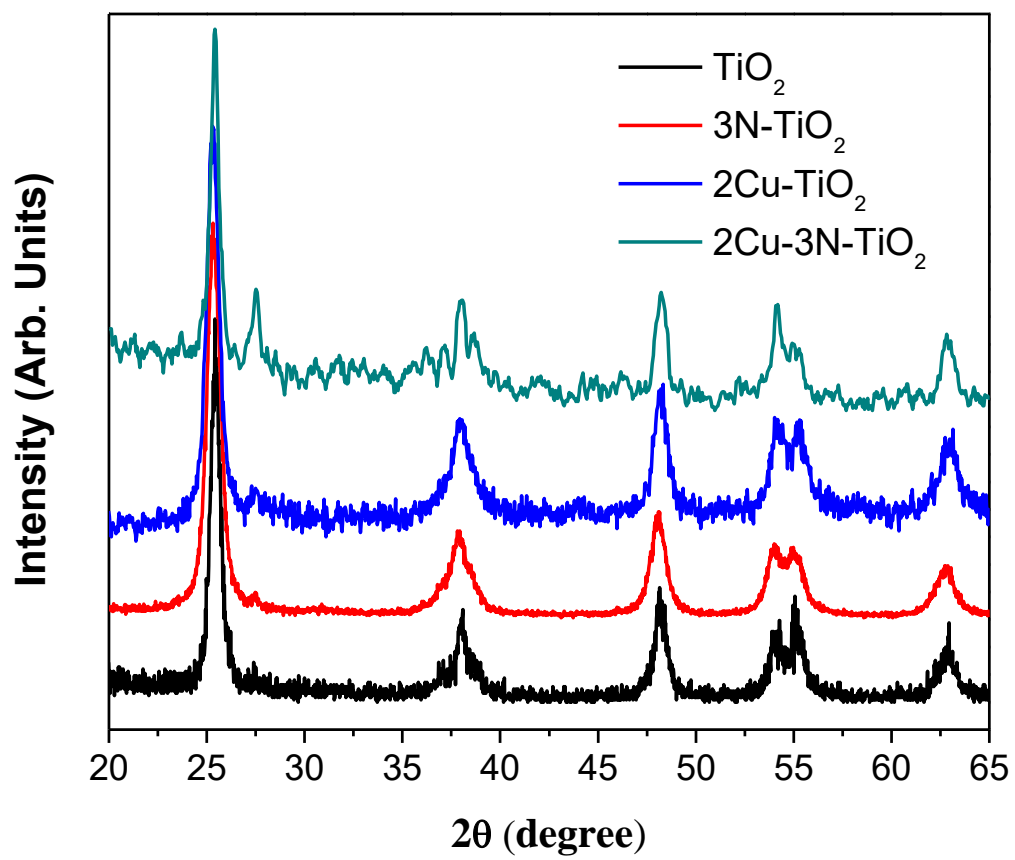
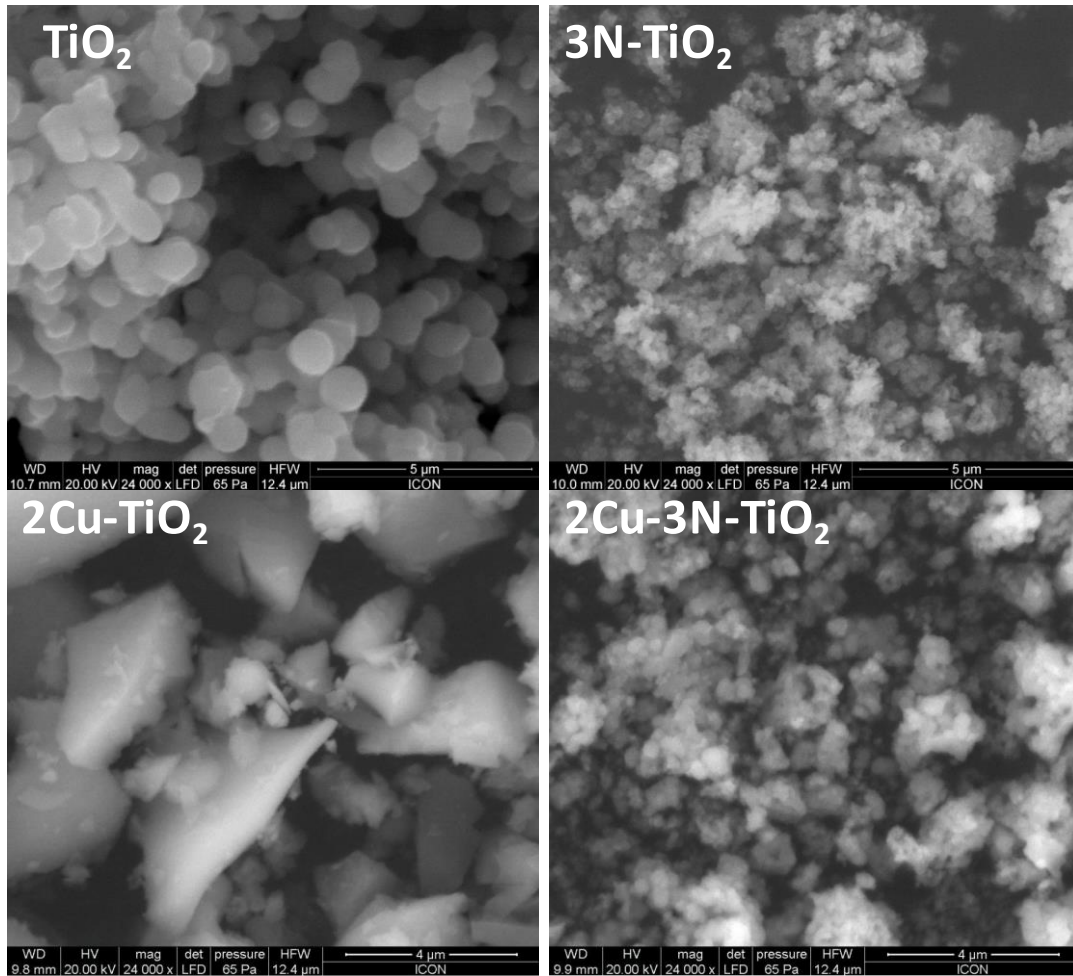
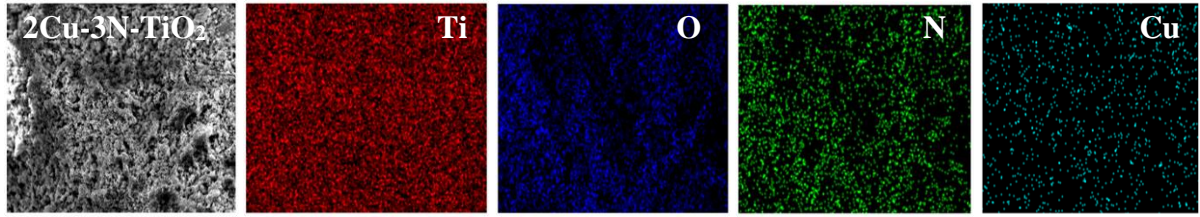


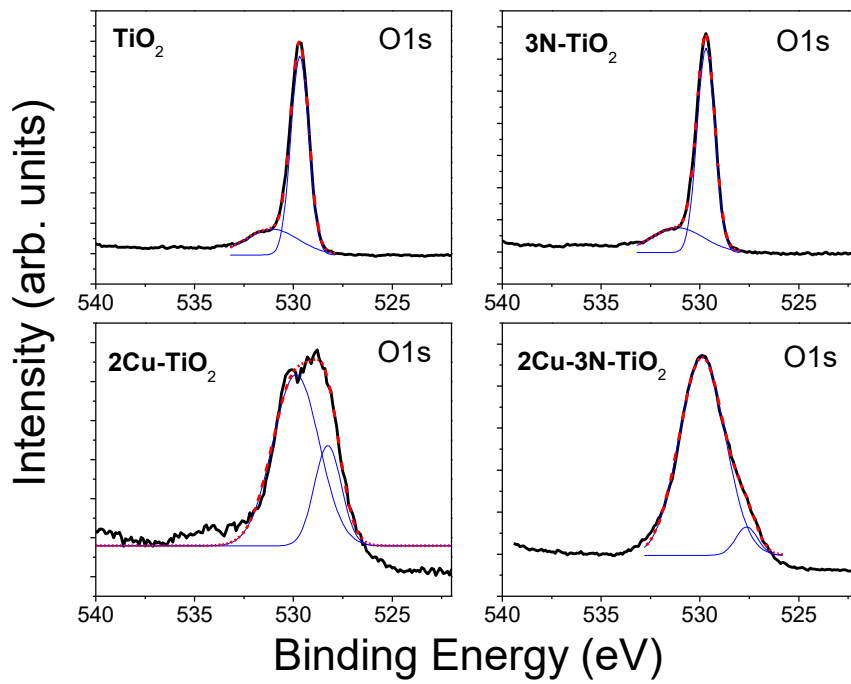
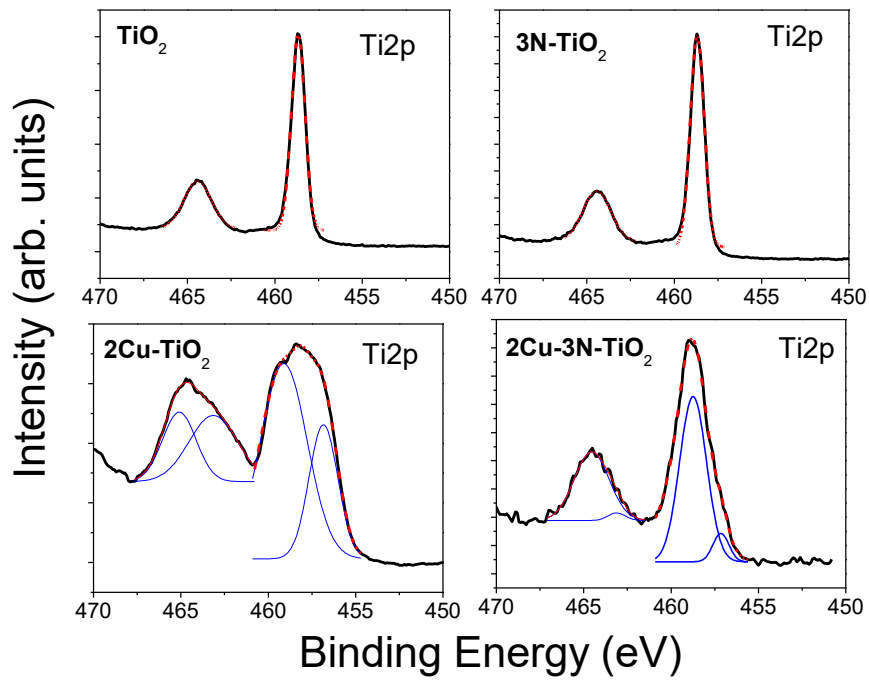
Figure 5:



**Figure 6:**



**Figure 7:**



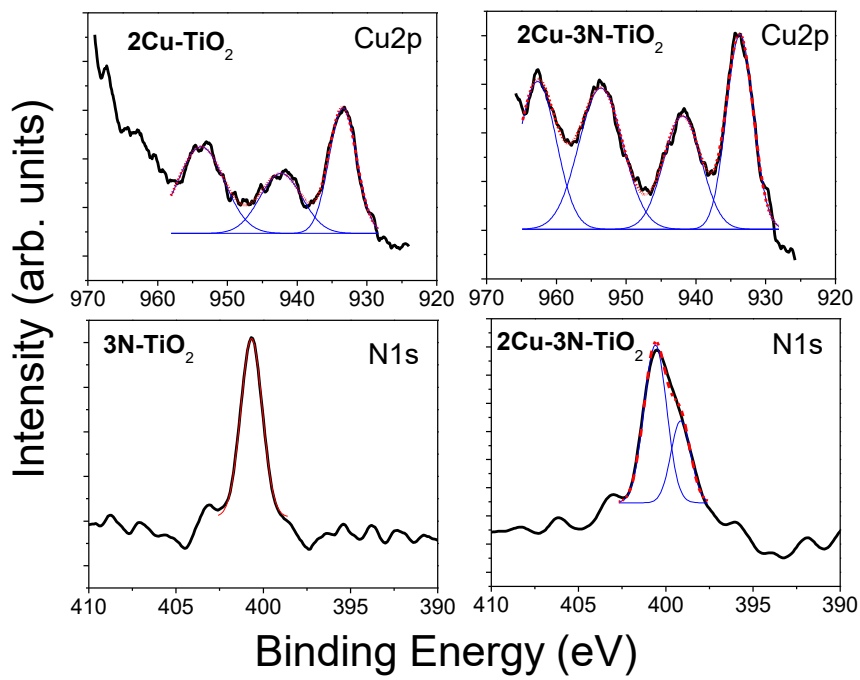


**Figure 8:**

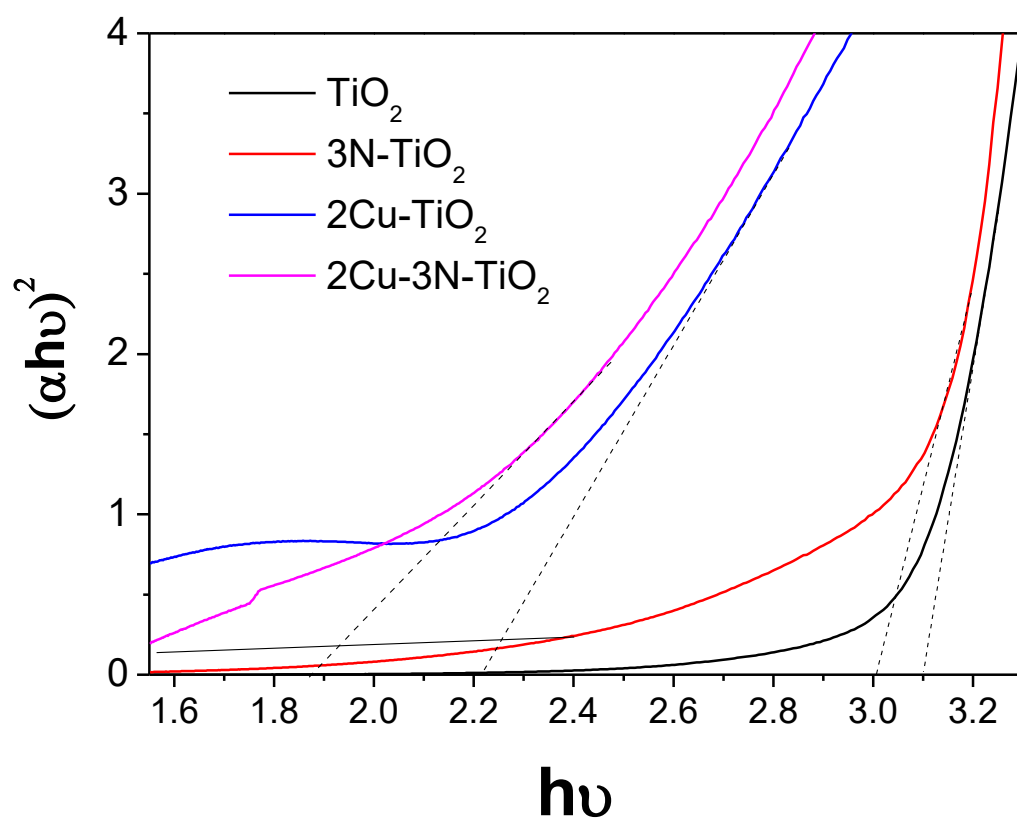


**Figure 9:**

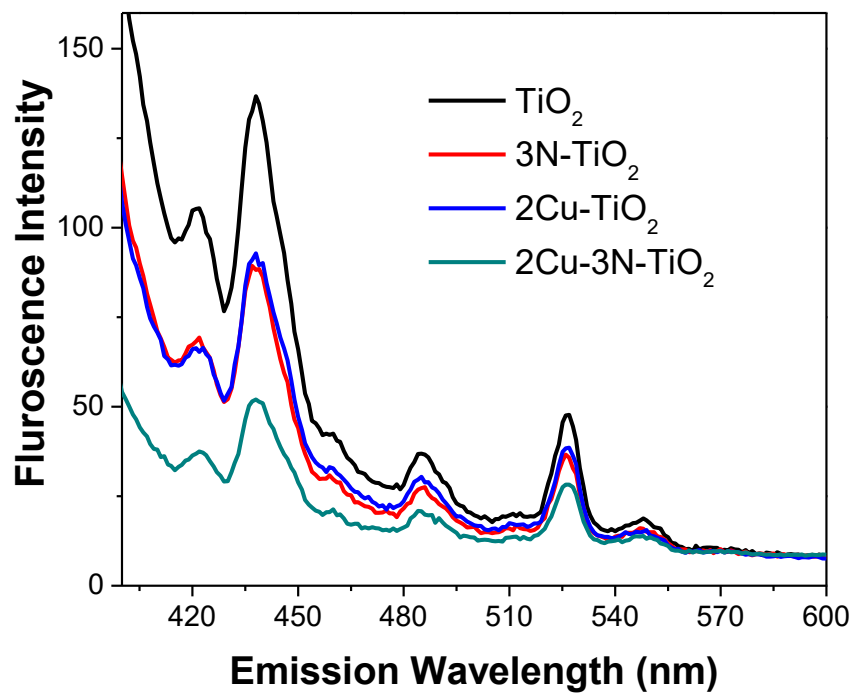


Figure 10:



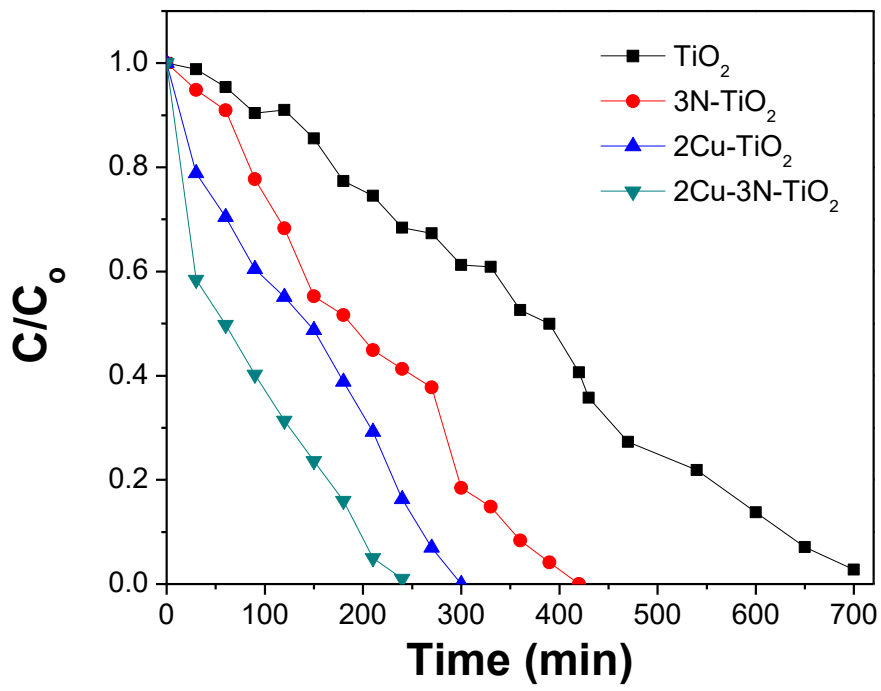


Figure 11:

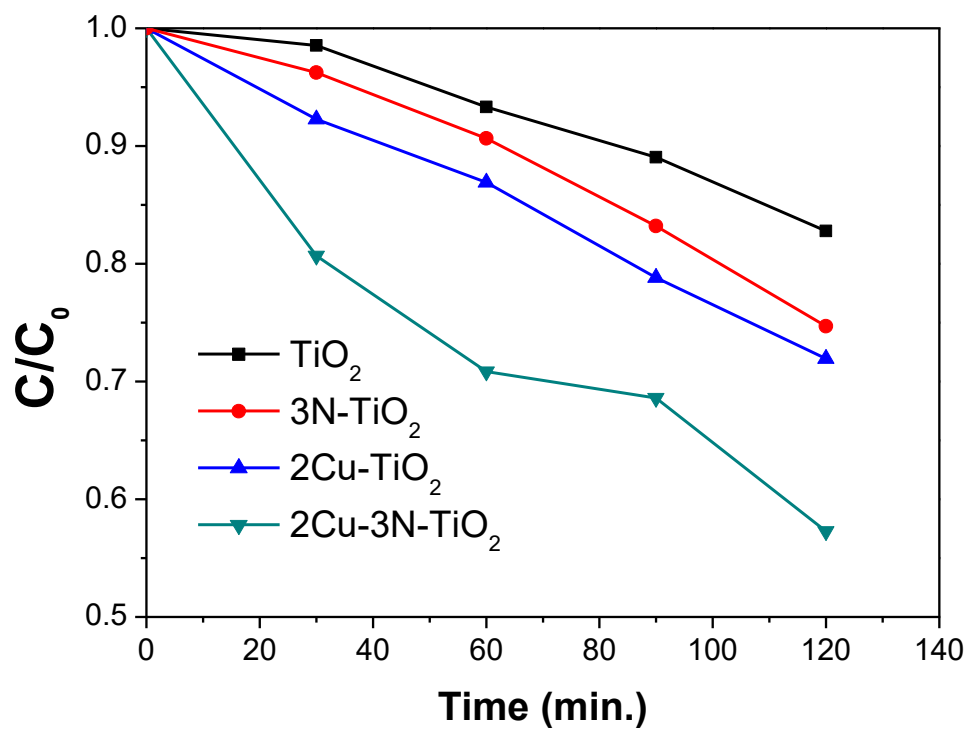


Figure12:

**Table 1:** Crystallite size and energy band gap of undoped, Cu-doped, N-doped, and 2Cu-3N-codoped TiO<sub>2</sub> powders.

<b>Sample</b>	<b>Band gap (eV)</b>	<b>Grain Size (nm)</b>
TiO <sub>2</sub>	3.15	10
TiO <sub>2</sub> -N 1%	3.1	12.84
TiO <sub>2</sub> -N 2%	3.05	11.84
TiO <sub>2</sub> -N 3%	3.0	15.20
TiO <sub>2</sub> -Cu 0.5%	2.6	6.61
TiO <sub>2</sub> -Cu 1%	2.4	15.28
TiO <sub>2</sub> -Cu 2%	2.2	10.25
TiO <sub>2</sub> -2%Cu -3%N	<2.0	13.04

**Table 2:** Photocatalytic activity of pure TiO<sub>2</sub>, 3N-TiO<sub>2</sub>, 2Cu-TiO<sub>2</sub> and 2Cu-3N-TiO<sub>2</sub> powders for Methylene Blue dye and p-Nitro Phenol degradation.

---

<b>Photocatalyst</b>	<b>Methylene Blue dye degradation</b>	<b>p-Nitro Phenol degradation</b>
----------------------	---------------------------------------	-----------------------------------

---

<b>Powders</b>				
	Apparent rate constant (min <sup>-1</sup> )	Degradation rate (mol/h/g of photocatalyst)	Apparent rate constant (min <sup>-1</sup> )	Degradation rate (mol/h/g of photocatalyst)
<b>TiO<sub>2</sub></b>	0.0046	3.83 x 10 <sup>-3</sup>	0.0016	1.33 x 10 <sup>-3</sup>
<b>3N-TiO<sub>2</sub></b>	0.0072	6.02 x 10 <sup>-3</sup>	0.0024	2.03 x 10 <sup>-3</sup>
<b>2Cu-TiO<sub>2</sub></b>	0.0082	6.88 x 10 <sup>-3</sup>	0.0027	2.27 x 10 <sup>-3</sup>
<b>3N-2Cu-TiO<sub>2</sub></b>	0.0140	11.67 x 10 <sup>-3</sup>	0.0043	3.55 x 10 <sup>-3</sup>

## **Copper and Nitrogen co-doped TiO<sub>2</sub> photocatalyst with enhanced optical absorption and catalytic activity**

**R. Jaiswal<sup>a</sup>, J. Bharambe<sup>a</sup>, N. Patel<sup>\*,a,b</sup>, Alpa Dashora<sup>a</sup>, D.C. Kothari<sup>a</sup> and A. Miotello<sup>b</sup>**

<sup>a</sup>*Department of Physics and National Centre for Nanosciences & Nanotechnology, University of Mumbai, Vidyanaagari, Santacruz (E), Mumbai 400 098, India*

<sup>b</sup>*Dipartimento di Fisica, Università degli Studi di Trento, I-38123 Povo ( Trento), Italy*

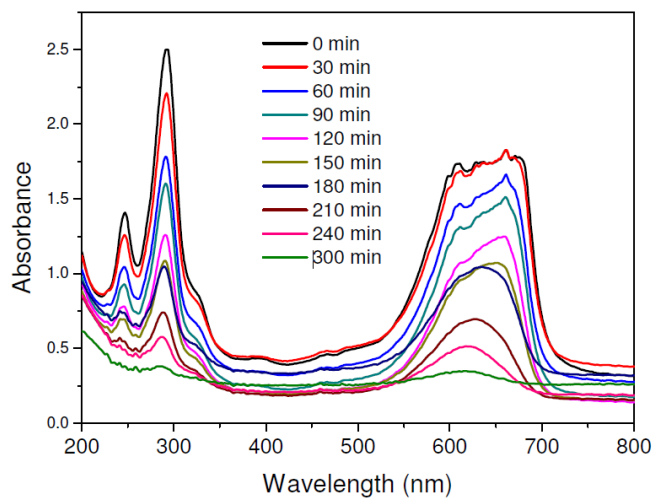


**Figure S1:** Photo-degradation of Methylene Blue dye solution in presence of TiO<sub>2</sub>-based photocatalyst

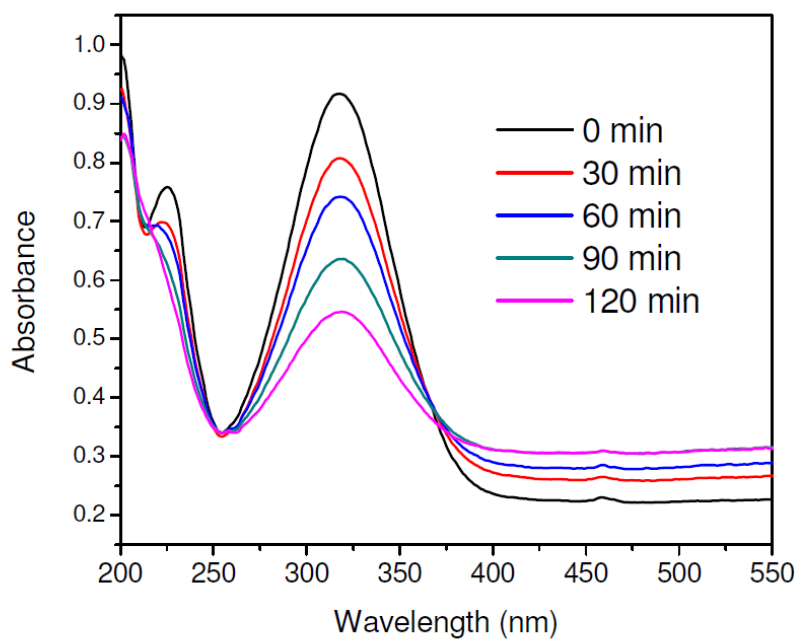


**Figure S2:** Photo-degradation of p-Nitro Phenol solution in presence of TiO<sub>2</sub>-based photocatalyst.